

# Intrinsic spin Hall effect from spin quantum metric

Longjun Xiang,<sup>1</sup> Hao Jin,<sup>1,\*</sup> and Jian Wang<sup>1,2,3,†</sup>

<sup>1</sup>College of Physics and Optoelectronic Engineering, Shenzhen University, Shenzhen 518060, China

<sup>2</sup>Department of Physics, The University of Science and Technology, Hefei, China

<sup>3</sup>Department of Physics, The University of Hong Kong, Pokfulam Road, Hong Kong, China

(Dated: June 5, 2024)

The intrinsic spin Hall effect (ISHE) proposed in [Sinova *et al.* *Phys. Rev. Lett.* **92**, 126603 (2004)] is driven by the spin Berry curvature. Herein, we establish the concept of *spin quantum metric*, which is the counterpart of the spin Berry curvature in the *spin quantum geometric tensor* defined in a similar way to the quantum geometric tensor. Dual to the  $\mathcal{T}$ -even ( $\mathcal{T}$ , time reversal) spin Berry curvature, the spin quantum metric features a  $\mathcal{T}$ -odd characteristic. Notably, we show that the  $\mathcal{T}$ -odd spin quantum metric can also drive an ISHE ( $\mathcal{T}$ -odd ISHE) under a high-frequency electric field. Guided by symmetry, we evaluate this  $\mathcal{T}$ -odd ISHE in the magnetically tilted surface Dirac cone and in ferromagnetic monolayer MnBi<sub>2</sub>Te<sub>4</sub>. We find that this  $\mathcal{T}$ -odd ISHE dominates when the Fermi level is close to the band (anti)crossing point, where its magnitude can be as large as the  $\mathcal{T}$ -even ISHE when an infrared driving field is applied. Our work not only uncovers an indispensable ingredient in the emergent community of quantum geometric physics but also offers a novel mechanism for ultrafast spintronics.

**Introduction.**— Quantum geometry received much attention recently [1–23], especially in the studies of Hall effect [1–14]. Usually, the quantum geometry property in the Hilbert space of Bloch electrons is associated with the non-Abelian Berry connection [16]  $\mathcal{A}_{nm}^\alpha(\mathbf{k}) = \langle \psi_n(\mathbf{k}) | i\partial_\alpha | \psi_m(\mathbf{k}) \rangle$ , where  $|\psi_n(\mathbf{k})\rangle$  is the quantum wavefunction of Bloch electrons and  $\partial_\alpha = \partial/\partial k_\alpha$  with  $k_\alpha$  being the crystal momentum. For instance, the gauge-invariant combination of  $\mathcal{A}_{nm}^\alpha$  defines the local quantum geometric tensor

$$T_{nm}^{\alpha\beta} \equiv \mathcal{A}_{nm}^\alpha \mathcal{A}_{mn}^\beta = g_{nm}^{\alpha\beta} - \frac{i\Omega_{nm}^{\alpha\beta}}{2}, \quad (1)$$

where the antisymmetric part  $\Omega_{nm}^{\alpha\beta}$  and symmetric part  $g_{nm}^{\alpha\beta}$  represents the local Berry curvature and quantum metric, respectively. At an early time, it has been established that the  $\mathcal{T}$ -odd ( $\mathcal{T}$ , time reversal) Berry curvature is responsible for the intrinsic anomalous Hall effect (IAHE) [1] in ferromagnetic metals, see Fig. (1b). Recently, it was further realized that the  $\mathcal{T}$ -even quantum metric can also exhibit a critical role in various Hall effects of quantum materials [7–12] and can even induce an intrinsic displacement Hall effect [14] under an AC electric field, see Fig. (1a).

Besides charge, the spin degree of freedom of Bloch electrons can also appreciate the quantum geometry effect [24–28]. In particular, Eq.(1) can be formally generalized into

$$T_{nm}^{\alpha\beta;\gamma} \equiv \frac{v_{nm}^{\alpha;\gamma} v_{mn}^\beta}{\epsilon_{nm}^2} = g_{nm}^{\alpha\beta;\gamma} - \frac{i\Omega_{nm}^{\alpha\beta;\gamma}}{2}, \quad (2)$$

where  $v_{nm}^\beta \equiv \langle \psi_n(\mathbf{k}) | \hat{v}^\beta | \psi_m(\mathbf{k}) \rangle$  for  $n \neq m$  is the interband matrix element of velocity operator  $\hat{v}^\beta$  and  $\epsilon_{nm} = \epsilon_n - \epsilon_m$  with  $\epsilon_n$  being the band energy. In addition,  $v_{nm}^{\alpha;\gamma} = \langle \psi_n(\mathbf{k}) | \hat{v}^{\alpha;\gamma} | \psi_m(\mathbf{k}) \rangle / 2$  with  $\hat{v}^{\alpha;\gamma} =$

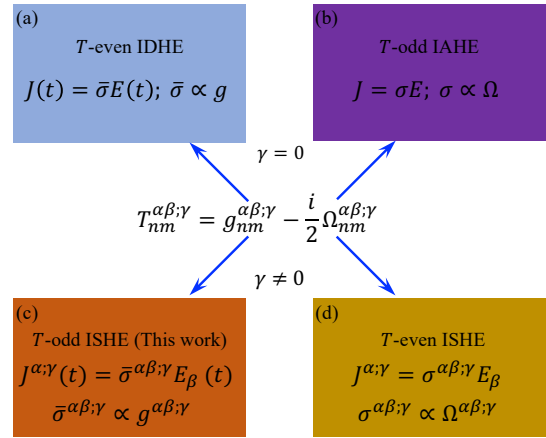


FIG. 1. The local quantum geometric tensor  $T_{nm}^{\alpha\beta;\gamma}$  probed by the linear responses of charge ( $\gamma = 0$ ) and spin ( $\gamma \neq 0$ ). (a) The intrinsic displacement Hall effect (IDHE) probes the  $\mathcal{T}$ -even quantum metric [14]. (b) The intrinsic anomalous Hall effect (IAHE) probes the  $\mathcal{T}$ -odd Berry curvature [1]. (c) The  $\mathcal{T}$ -odd intrinsic spin Hall effect (ISHE) probes the *spin quantum metric* (this work). (d) The  $\mathcal{T}$ -even ISHE probes the spin Berry curvature.

$(\hat{v}^\alpha \hat{s}^\gamma + \hat{s}^\gamma \hat{v}^\alpha) / 2$ , where  $\hat{s}^{\gamma=0} = e$  stands for the elementary charge and  $\hat{s}^{\gamma \neq 0} = \hbar \sigma^\gamma / 2$  the spin angular momentum operator. Here  $\sigma^\gamma$  with  $\gamma \in \{x, y, z\}$  is the Pauli matrix. Note that Eq.(2) reduces into Eq.(1) for  $\gamma = 0$  since  $v_{nm}^\alpha = i\epsilon_{nm} \mathcal{A}_{nm}^\alpha$  with  $n \neq m$ . As a result,  $T_{nm}^{\alpha\beta;\gamma}$  for  $\gamma \neq 0$  can be naturally defined as the local *spin quantum geometric tensor*, whose imaginary part  $\Omega_{nm}^{\alpha\beta;\gamma}$  gives the well-known spin Berry curvature while its real part  $g_{nm}^{\alpha\beta;\gamma}$  defines the *spin quantum metric* proposed in this work. Interestingly, although the spin Berry curvature was known as the quantum geometric origin of the intrinsic spin Hall effect (ISHE) proposed by Sinova *et al.*

[24], see Fig. (1d), whether its counterpart—*spin quantum metric* can induce an ISHE remains unknown.

In this *Letter*, by revisiting the linear response theory for spin current, we show that the spin quantum metric indeed can deliver an ISHE particularly under an AC electric field. Interestingly, due to the involvement of spin, we find that the spin quantum metric and the spin Berry curvature features the  $\mathcal{T}$ -odd ( $\mathcal{T}$ , time reversal) and  $\mathcal{T}$ -even characteristics, respectively; whereas the quantum metric and Berry curvature given in Eq. (1) features the  $\mathcal{T}$ -even and  $\mathcal{T}$ -odd property, respectively. Guided by symmetry, we evaluate this  $\mathcal{T}$ -odd ISHE in the magnetically tilted surface Dirac cone and in ferromagnetic monolayer MnBi<sub>2</sub>Te<sub>4</sub>. We find that this  $\mathcal{T}$ -odd ISHE dominates when the Fermi level is close to the band (anti)crossing point, in which its magnitude can be as large as the  $\mathcal{T}$ -even ISHE when an infrared driving field is applied. Our work not only establishes the concept of spin quantum metric but also offers a novel mechanism for ultrafast spintronics.

**The linear response theory.**— To derive the *spin quantum metric* and the spin Berry curvature on the same theoretical footing, we first develop the linear response theory for spin current under an AC electric field. Instead of using the Green's function approach [29], we iteratively solve the quantum Liouville equation and obtain the off-diagonal density matrix element at the first order of the electric field ( $e = \hbar = 1$ ) [14]

$$\rho_{mn}^{(1)} = \frac{1}{2} \sum_{\omega_1} \frac{f_{nm} \mathcal{A}_{mn}^{\alpha}}{\omega_1 - \epsilon_{mn} + i\eta} E_{\alpha} e^{-i(\omega_1 + i\eta)t}, \quad (3)$$

where  $\omega_1 = \pm\omega$  with  $\omega$  the driving frequency,  $f_{nm} = f_n - f_m$  with  $f_n$  being the equilibrium Fermi distribution function, and  $\eta$  is an infinitesimal quantity. Note that the Einstein summation convention is assumed for the repeated Greek alphabet here and hereafter. With Eq.(3), the linear spin current density defined by  $J^{\alpha;\gamma} \equiv -\sum_{mn} \int_k v_{nm}^{\alpha;\gamma} \rho_{mn}^{(1)}$  can be directly calculated as

$$J^{\alpha;\gamma} = -\frac{1}{2} \sum_{\omega_1} \sum_{mn} \int_k \frac{f_{nm} v_{nm}^{\alpha;\gamma} \mathcal{A}_{mn}^{\beta}}{\omega_1 - \epsilon_{mn}} E_{\beta} e^{-i\omega_1 t}, \quad (4)$$

where  $\int_k = \int d\mathbf{k}/(2\pi)^d$  with  $d$  being the spatial dimension and we set  $\eta = 0$  since we are interested in the nonresonant response with  $\epsilon_{mn} \neq \hbar\omega$ . Furthermore, using  $-1/(\omega_1 - \epsilon_{mn}) = 1/\epsilon_{mn} - \omega_1/[\epsilon_{mn}(\omega_1 - \epsilon_{mn})]$  and  $\mathcal{A}_{mn}^{\beta} = -iv_{mn}^{\beta}/\epsilon_{mn}$  when  $m \neq n$ , we find that Eq.(4) can be partitioned into  $J^{\alpha;\gamma} = J_{DC}^{\alpha;\gamma} + J_{AC}^{\alpha;\gamma}$ , where

$$J_{DC}^{\alpha;\gamma} = \sum_{\omega_1} \sum_{mn} \int_k \frac{-if_{nm} v_{nm}^{\alpha;\gamma} v_{mn}^{\beta}}{2\epsilon_{mn}^2} E_{\beta} e^{-i\omega_1 t}, \quad (5)$$

$$J_{AC}^{\alpha;\gamma} = \sum_{\omega_1} \sum_{mn} \int_k \frac{i\omega_1 f_{nm} v_{nm}^{\alpha;\gamma} v_{mn}^{\beta}}{2\epsilon_{mn}^2 (\omega_1 - \epsilon_{mn})} E_{\beta} e^{-i\omega_1 t}. \quad (6)$$

We wish to remark that Eq.(5) is nothing but the linear conduction spin current density, which can survive in DC limit ( $\omega \rightarrow 0$ ) and is fully determined by the spin Berry curvature. To see that, by interchanging the dummy indices, we find that Eq.(5) becomes

$$J_{DC}^{\alpha;\gamma} = \sum_n \int_k f_n \Omega_n^{\alpha\beta;\gamma} E_{\beta} \cos(\omega t), \quad (7)$$

where the frequency summation has been performed and  $\Omega_{nm}^{\alpha\beta;\gamma}$  has been defined in Eq.(2). We wish to mention that Eq.(7) usually is derived with Kubo formula at the clean limit [29] where the current due to Eq.(6) usually is overlooked.

Similar to the linear response theory for charge, Eq.(6) also gives the displacement spin current density, which can only survive in AC transport ( $\omega \neq 0$ ) and can be expressed as  $J_{AC}^{\alpha;\gamma} = \partial_t P^{\alpha;\gamma}(t)$ , where  $P^{\alpha;\gamma}(t)$  is the spin polarization given by

$$P^{\alpha;\gamma} = \sum_n \int_k f_n [\mathcal{G}_n^{\alpha\beta;\gamma} \cos(\omega t) + \mathcal{F}_n^{\alpha\beta;\gamma} \sin(\omega t)] E_{\beta},$$

obtained by both the index interchanging and summation over  $\omega_1$ . Here

$$\mathcal{G}_n^{\alpha\beta;\gamma} = \sum_{m \neq n} \Pi_{mn}^1(\omega) g_{nm}^{\alpha\beta;\gamma}, \quad (8)$$

$$\mathcal{F}_n^{\alpha\beta;\gamma} = \sum_{m \neq n} \Pi_{mn}^2(\omega) \Omega_{nm}^{\alpha\beta;\gamma}, \quad (9)$$

where  $\Pi_{mn}^1(\omega) = \epsilon_{mn}/(\omega^2 - \epsilon_{mn}^2)$  and  $\Pi_{mn}^2(\omega) = \omega^2/(\omega^2 - \epsilon_{mn}^2)$ . By comparing with Eq. (2), it is easy to see that  $\mathcal{G}_n^{\alpha\beta;\gamma}$  and  $\mathcal{F}_n^{\alpha\beta;\gamma}$  encode the information of the spin quantum metric and spin Berry curvature, respectively. Importantly,  $\mathcal{G}_n^{\alpha\beta;\gamma}$  ( $\mathcal{F}_n^{\alpha\beta;\gamma}$ ) exactly shows the same symmetry transformation as  $g_{nm}^{\alpha\beta;\gamma}$  ( $\Omega_{nm}^{\alpha\beta;\gamma}$ ) and is termed as the band-normalized spin quantum metric (spin Berry curvature) following Ref. [43], where the weight factor  $\Pi_{mn}^i(\omega)$  can only affect its magnitude. Below we focus on  $\mathcal{G}_n^{\alpha\beta;\gamma}$  since we are interested in the spin quantum metric throughout this work.

The same as the spin Berry curvature, the spin quantum metric can also induce an ISHE when the integral of  $\mathcal{G}_n^{\alpha\beta;\gamma}$  with  $\alpha \neq \beta$  over the occupied states does not vanish. In particular, by defining  $J_{AC}^{\alpha;\gamma} = \bar{\sigma}^{\alpha\beta;\gamma} E_{\beta} \sin(\omega t)$ , the corresponding ISHE conductivity can be written as

$$\bar{\sigma}^{\alpha\beta;\gamma} = \omega \sum_n \int_k f_n \mathcal{G}_n^{\alpha\beta;\gamma}. \quad (10)$$

This conductivity features a formal similarity with the spin Berry curvature induced ISHE conductivity [30], which can be extracted from Eq. (7) as

$$\sigma^{\alpha\beta;\gamma} = \sum_n \int_k f_n \Omega_n^{\alpha\beta;\gamma}. \quad (11)$$

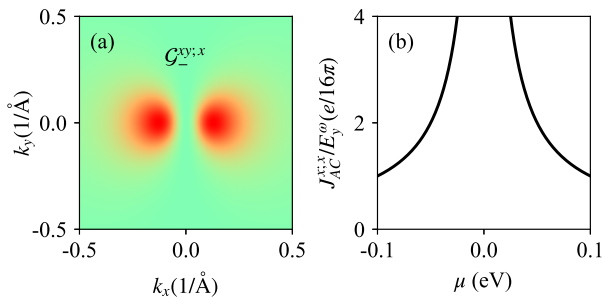


FIG. 2. (a) The  $\mathbf{k}$ -resolved distribution for the band-normalized spin quantum metric defined by Eq.(13). (b) The dependence of  $\mathcal{T}$ -odd ISHE spin current density on the chemical potential  $\mu$  in the unit of  $e/(16\pi)$ . Note that  $E_y^{\omega} = E_y \sin(\omega t)$ . Parameters:  $t_x/\hbar v = 10$ ,  $\hbar\omega = 10\text{meV}$ .

At this stage, we remark that Eq. (10) and Eq. (11), respectively, features the  $\mathcal{T}$ -odd and  $\mathcal{T}$ -even property due to  $\mathcal{T}\mathcal{G}_n^{\alpha\beta;\gamma} = -\mathcal{G}_n^{\alpha\beta;\gamma}$  and  $\mathcal{T}\Omega_n^{\alpha\beta;\gamma} = \Omega_n^{\alpha\beta;\gamma}$ , which is due to  $\mathcal{T}v_{nm}^{\alpha;\gamma} = v_{mn}^{\alpha;\gamma}$  and  $\mathcal{T}v_{nm}^{\beta} = -v_{mn}^{\beta}$ . In addition, we mention that the Berry curvature and quantum metric given by Eq. (1), respectively, shows the  $\mathcal{T}$ -odd and  $\mathcal{T}$ -even behavior due to  $\mathcal{T}\mathcal{A}_{nm}^{\alpha} = \mathcal{A}_{mn}^{\alpha}$ , as compared in Fig. (1). Finally, we stress that Eq. (10) can only appear in AC transport while Eq. (11) can appear in DC ( $\omega \rightarrow 0$ ) transport. To close this section, we conclude that Eq.(10), together with Eq.(8) which encodes the spin quantum metric, is the main result of this *Letter*.

*A model study.*— To acquire a quick understanding of the spin quantum metric, we first apply our theory to the surface Dirac cone of topological insulator that is tilted by an in-plane magnetic field, which can be described by the following two-band effective Hamiltonian [37],

$$H = \mathbf{t} \cdot \mathbf{k} + v(k_x \sigma_y - k_y \sigma_x), \quad (12)$$

where  $v$  is the Fermi velocity and  $\mathbf{t} = (t_x, t_y)$  is the tilt vector. With Eq.(8) by assuming that  $\epsilon_{mn} \gg \hbar\omega$ , we find that the band-normalized spin quantum metric that is even in  $k_a$  is given by

$$\mathcal{G}_{\pm}^{xy;x} = \mp \frac{t_x k_x^2}{4v^2 k^5}, \quad (13)$$

where  $+$ ( $-$ ) stands for the upper (lower) band and  $k^2 = k_x^2 + k_y^2$ . This result shows a dipole landscape in the  $k_x$ - $k_y$  plane, as shown in Fig. (2a). As a result, the band-normalized spin quantum metric can induce an collinear ISHE (defined below) and the corresponding conductivity at zero temperature for  $\mu < 0$  can be calculated as

$$\bar{\sigma}^{xy;x} = \int_k \Theta(\mu - \epsilon_-) \frac{t_x k_x^2}{4v^2 k^5} = -\frac{t_x}{16\pi v \mu}, \quad (14)$$

where  $\Theta$  is the step function and the polar coordinate  $\mathbf{k} = k(\cos \theta, \sin \theta)$  has been used to obtain the final result.

Furthermore, the  $\mathcal{T}$ -odd spin Hall current then is given by

$$J_{AC}^{x;x} = \frac{e}{16\pi} \frac{t_x}{\hbar v} \frac{\hbar\omega}{|\mu|} E_y \sin(\omega t), \quad (15)$$

where  $e$  and  $\hbar$  are restored by dimension analysis and we have also taken into account the case of  $\mu > 0$ .

We wish to remark that the  $\mathcal{T}$ -odd ISHE conductivity is no longer universal like its  $\mathcal{T}$ -even counterpart [24]. In particular, we note that the spin Berry curvature that is even  $k_a$  is given by

$$\Omega_{\pm}^{xy;z} = \pm \frac{k_x^2}{4v k^5}, \quad (16)$$

which almost shows the same landscape on the  $k_x$ - $k_y$  plane with the spin quantum metric. Note that the survived spin quantum metric and spin Berry curvature have a different spin polarization. As a result, by inserting this expression into Eq.(11) and performing a similar calculation, we find that

$$J_{DC}^{x;z} = -\frac{e}{16\pi} E_y \cos(\omega t), \quad (17)$$

which shows a universal behavior like with the two-dimensional Rashba electron gas [24], as expected.

By taking the  $\mathcal{T}$ -even universal conductivity as a benchmark, we further display the dependence of spin current on the chemical potential  $\mu$  in Fig. (2b). Notably, by taking  $t_x/(\hbar v) \sim 10$ , we find that the  $\mathcal{T}$ -odd ISHE driving by a THz field ( $\hbar\omega \sim 10\text{meV}$ ) can be the same order as the  $\mathcal{T}$ -even counterpart. Notably, the  $\mathcal{T}$ -odd ISHE can be further enhanced when the chemical potential  $\mu$  is approaching the band crossing point.

*Symmetry analysis.*— In addition to the model calculations, we next apply our theory to investigate the spin quantum metric driven ISHE in realistic materials. Before proceeding, we note that the  $\mathcal{T}$ -even and  $\mathcal{T}$ -odd ISHE conductivity tensors can possess both the longitudinal and transverse components[41], in stark contrast with the IAHE conductivity tensor that just contains the transverse component. Throughout this work, we focus on the transverse responses. In particular, following Ref. [41], for the  $\mathcal{T}$ -odd ISHE conductivity  $\bar{\sigma}^{\alpha\beta;\gamma}$  with  $\alpha \neq \beta \neq \gamma$  we will call it the conventional  $\mathcal{T}$ -odd ISHE; for the  $\mathcal{T}$ -odd conductivity  $\bar{\sigma}^{\alpha\beta;\gamma}$  with  $\alpha \neq \beta$  and  $\gamma \in \{\alpha, \beta\}$  we will call it the collinear  $\mathcal{T}$ -odd ISHE. Furthermore, the same as the  $\mathcal{T}$ -even ISHE, the  $\mathcal{T}$ -odd ISHE can also feature different tensor shape under the magnetic point group (MPG) symmetry.

To obtain that, we first note that all the 32 grey MPGs with  $\mathcal{T}$ -symmetry (1') can not support the  $\mathcal{T}$ -odd ISHE. Additionally, we find that Eq.(10) in fact is a  $\mathcal{PT}$ -odd

TABLE I. The magnetic point groups for the conventional (for  $\bar{\sigma}^{\alpha\beta;\gamma}, \alpha \neq \beta \neq \gamma$ ) and collinear (for  $\bar{\sigma}^{\alpha\beta;\gamma}, \alpha \neq \beta$  and  $\gamma \in \{\alpha, \beta\}$ )  $\mathcal{T}$ -odd ISHE, respectively.

$\bar{\sigma}^{\alpha\beta;\gamma}$	Magnetic point groups
$\alpha \neq \beta \neq \gamma$	1, $\bar{1}$ , 2, $m$ , $2/m$ ,
	3, $\bar{3}$ , 222, $mm2$ , $mmm$ ,
	4', $\bar{4}'$ , $4'/m$ , 32, $3m$ ,
	$\bar{3}m$ , 422, $4mm$ , $\bar{4}2m$ , $4/mmm$ ,
	622, $6mm$ , $\bar{6}m2$ , $6/mmm$ , $\bar{4}'2m'$ ,
	$4'2'2'$ , 23, $m\bar{3}$ , 432, $\bar{4}3m$ ,
	$m\bar{3}m'$ , $4'32'$ , $\bar{4}'3m'$ , $m\bar{3}m'$ ,
	1, $\bar{1}$ , 2, $m$ , $2/m$ ,
	2', $m'$ , $2'/m'$ , 3, $\bar{3}$ ,
	$2'2'2'$ , $m'm'2$ , $m'm'm$ , $m'm'2'$ ,
4, $\bar{4}$ , $4/m$ , 6,	
$\bar{6}$ , $6/m$ , 4', $\bar{4}'$ ,	
4'/m, 32', 3m', $\bar{3}m'$ ,	
$4'2'2'$ , $4m'm'$ , $\bar{4}2'm'$ , $4/mmm'm'$ ,	
$6'2'2'$ , $6m'm'$ , $\bar{6}m'2'$ , $6/mmm'm'$ ,	
$4'm'm$ , $\bar{4}'2'm$ , $4'/mm'm$ , 6',	
$\bar{6}'$ , $6'/m'$ , $\bar{6}'m'2'$ ,	

tensor because of  $\mathcal{P}\bar{\sigma}^{\alpha\beta;\gamma} = \bar{\sigma}^{\alpha\beta;\gamma}$ . As a result, out of the 90 MPGs without  $\mathcal{T}$ -symmetry, 21 of them with  $\mathcal{PT}$  symmetry ( $-1'$ ) [42] can also not support this ISHE. Finally, for the remaining 69 MPGs, we can resort to the Neumann principle

$$\bar{\sigma}^{\alpha\beta;\gamma} = \eta_T \det(R) R_{\alpha\alpha'} R_{\beta\beta'} R_{\gamma\gamma'} \sigma^{\alpha'\beta';\gamma'} \quad (18)$$

to acquire the specific tensor shape of  $\bar{\sigma}^{\alpha\beta;\gamma}$ . In Eq.(18),  $\eta_T = +(-)$  is responsible for the symmetry operation  $R$  ( $RT$ ),  $\det(R)$  stands for the determinant of  $R$ , and  $R_{\alpha\alpha'}$  is the matrix element of  $R$ . Note that Eq.(18) has been implemented in the online Bilbao database. As a result, by defining the Jahn notation  $aeV^3$  for the  $\mathcal{T}$ -odd rank-3 pseudotensor  $\bar{\sigma}^{\alpha\beta;\gamma}$ , we can obtain the tensor shape of  $\bar{\sigma}^{\alpha\beta;\gamma}$  once for all, see Supplemental Material [44]. Interestingly, we find that some of the 69 MPGs can only support either the conventional  $\mathcal{T}$ -odd ISHE or the collinear  $\mathcal{T}$ -odd ISHE and some of them can support both, as summarized in Table I.

As a comparison, we wish to mention that the spin Berry curvature induced ISHE corresponds to a  $\mathcal{T}$ -even rank-3 pseudotensor, whose Jahn notation is  $eV^3$ , which has also been used to classify the conventional and collinear  $\mathcal{T}$ -even ISHE [41]. Armed with the symmetry analysis, we are now ready to evaluate the  $\mathcal{T}$ -odd ISHE in realistic materials by combining our theory with first-principles calculation.

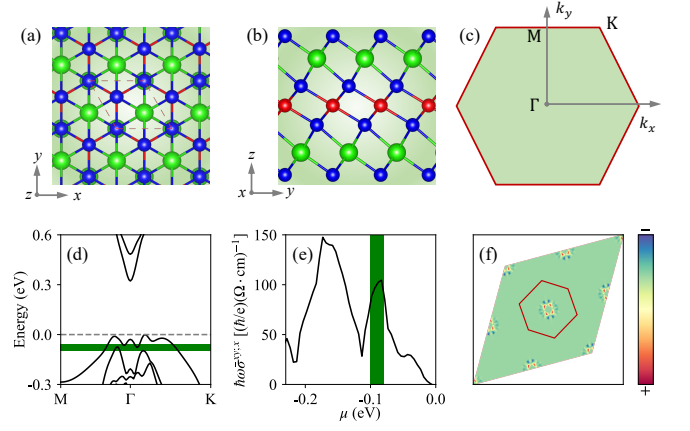


FIG. 3. (a) The top view of monolayer  $\text{MnBi}_2\text{Te}_4$ . Here the red dashed line indicates the primitive unit cell. (b) The side view of monolayer  $\text{MnBi}_2\text{Te}_4$ . Along  $z$  direction, the typical Te-Bi-Te-Mn-Te-Bi-Te septuple structure is shown. (c) The first Brillouin zone. (d) The band structure of monolayer  $\text{MnBi}_2\text{Te}_4$ . Here the horizontal dashed line and green shadow indicates the Fermi level and band anticrossing, respectively. (e) The dependence on the chemical potential  $\mu$  for the  $\mathcal{T}$ -odd ISHE conductivity. (f) The  $\mathbf{k}$ -resolved distribution for the spin quantum metric.

**A material study.**— Guided by symmetry, we next consider a realistic ferromagnetic monolayer  $\text{MnBi}_2\text{Te}_4$  by combining our theory with first-principles calculation. The monolayer  $\text{MnBi}_2\text{Te}_4$  has been experimentally fabricated from its van der Waals bulk crystal. The crystal structure of monolayer  $\text{MnBi}_2\text{Te}_4$  is displayed in Fig. 3a (top view) and 3b (side view). Like monolayer graphene and monolayer  $\text{MoS}_2$ , from Fig. 3a we find that the monolayer  $\text{MnBi}_2\text{Te}_4$  also features a hexagonal lattice, which is described by the space group  $P\bar{3}m1$  (No. 164) and point group  $3m(D_{3d})$  without the consideration of the magnetic order. As a result, the primitive cell of the monolayer  $\text{MnBi}_2\text{Te}_4$  can be chosen as a parallelogram (indicated by the red dashed line in Fig. 3a) and the corresponding first Brillouin zone is shown in Fig. 3c. Meanwhile, Fig. 3b clearly exhibits the typical Te-Bi-Te-Mn-Te-Bi-Te septuple structure of monolayer  $\text{MnBi}_2\text{Te}_4$ . By further taking into account the magnetic order from the Mn atom, the monolayer  $\text{MnBi}_2\text{Te}_4$  in fact possesses a magnetic point group of  $\bar{3}m'$ , which allows the  $\mathcal{T}$ -odd collinear ISHE in terms of Table I.

In Fig. 3d, we show the band structure of monolayer  $\text{MnBi}_2\text{Te}_4$  (see Ref.[44] for the computation details), which shows a narrow gap semiconductor, consistent with previous studies [25]. Note that two anticrossing points appearing near  $-0.1$  eV have been shown as the physical origin of large nonlinear spin polarization [25]. Interestingly, by calculating the collinear  $\mathcal{T}$ -odd ISHE conductivity  $\bar{\sigma}^{xy;x}$ , we find that the same anticrossing points also leads to a strong ISHE peak, as shown in Fig. 3e. Furthermore, by plotting the  $\mathbf{k}$ -resolved

intergrand at energy cut near  $-0.1$  eV, we find that the hotspot of spin quantum metric is near  $\Gamma$  point, as shown in Fig. 3f. This further confirms our observation. Note that in Fig. 3e, we set  $\hbar\omega = 0.1$ eV (an AC electric field with an infrared frequency) and we find that *spin quantum metric* induced ISHE can be the same order as the  $\mathcal{T}$ -even ISHE.

*Discussion and summary.*— We wish to remark that the  $\mathcal{T}$ -odd ISHE driving by the spin quantum metric under an AC electric field is different from the previously studied  $\mathcal{T}$ -odd spin Hall effect [38–40], which can survive in DC limit and all of them features the extrinsic nature. In addition, we mention that the measurements of spin Hall effect can be easily accessible with state-of-art technique, such as the time-resolved magnetic-optical Kerr effect (tMOKE), and a time-dependent spin accumulation can be expected in terms of our proposal. In summary, by developing the linear response theory for spin current, we show that the spin quantum metric can induce a  $\mathcal{T}$ -odd ISHE under an AC electric field. Since the spin quantum metric is the quantum geometric counterpart of the  $\mathcal{T}$ -even spin Berry curvature, thereby the ISHE driven by spin quantum metric can only appear in  $\mathcal{T}$ -broken systems, as illustrated in the magnetically tilted surface Dirac cone and in a realistic ferromagnetic material  $\text{MnBi}_2\text{Te}_4$ . We find that the  $\mathcal{T}$ -odd ISHE dominates when the Fermi level is near the band (anti)crossing point that usually caused by spin-orbital coupling, where its magnitude can be as large as the  $\mathcal{T}$ -even ISHE under a THz or infrared driving field.

Our work establishes the concept of spin quantum metric for the first time from the perspective of quantum geometry and may offer a promising mechanism to the ultrafast spintronics [31]. In addition, we wish to mention that the dynamical  $\mathcal{T}$ -odd ISHE particularly with an in-plane spin polarization may offer a desirable way to engender spin-orbit torque in 2D materials with an out-of-plane magnetization. Finally, although we focus on the spin degree of freedom, the theoretical formulation used in this work can be easily extended to study the high-frequency orbital angular momentum accumulation-dynamical orbital Hall effect, which may be explored in the future.

## ACKNOWLEDGEMENTS

J. W. thanks the financial support from the National Natural Science Foundation of China (Grant No. 12034014).

---

\* jh@szu.edu.cn

- <sup>†</sup> jianwang@hku.hk
- [1] D. Xiao, M.-C. Chang, and Q. Niu, *Rev. Mod. Phys.* **82**, 1959 (2010).
  - [2] I. Sodemann and L. Fu, *Phys. Rev. Lett.* **115**, 216806 (2015).
  - [3] Q. Ma, S.-Y. Xu, H. Shen, D. MacNeill, V. Fatemi, T.-R. Chang, A. M. M. Valdivia, S. F. Wu, Z. Du, C.-H. Hsu, S. Fang, Q. D. Gibson, K. Watanabe, T. Taniguchi, R. J. Cava, E. Kaxiras, H.-Z. Lu, H. Lin, L. Fu, N. Gedik, and P. Jarillo-Herrero, *Nature* **565**, 337 (2019).
  - [4] K. F. Kang, T. X. Li, E. Sohn, J. Shan, and K. F. Mak, *Nat. Mater.* **18**, 324 (2019).
  - [5] C.-P. Zhang, X.-J. Gao, Y.-M. Xie, H. C. Po, and K. T. Law, *Phys. Rev. B* **107**, 115142 (2023).
  - [6] Z. Z. Du, H.-Z. Lu, and X. C. Xie, *Nat. Rev. Phys.* **3**, 744 (2021).
  - [7] Y. Gao, S. Y. A. Yang, and Q. Niu, *Phys. Rev. Lett.* **112**, 166601 (2014).
  - [8] A. Gao *et al.*, *Science* **381**, 181 (2023).
  - [9] N.-Z. Wang, D. Kaplan, Z.-W. Zhang, T. Holder, N. Cao, A.-F. Wang, X.-Y. Zhou, F.-F. Zhou, Z.-Z. Jiang, C.S. Zhang, S.-H. Ru, H.-B. Cai, K. Watanabe, T. Taniguchi, B.-H. Yan and W.-B. Gao, *Nature (London)* **621**, 487 (2023).
  - [10] J. Han, T. Uchimura, Y. Araki, J.-Y. Yoon, Y. Takeuchi, Y. Yamane, S. Kanai, J. Ieda, H. Ohno, and S. Fukami, *Nat. Phys.* (2024).
  - [11] L. J. Y. Wang, J. J. Zhu, H. Chen, H. Wang, J. Liu, Y.-X. Huang, B. Y. Jiang, J. Zhao, H. Shi, G. Tian, H. Wang, Y. G. Yao, D. P. Yu, Z. W. Wang, C. Xiao, S. Y. A. Yang, and X. S. Wu, *Phys. Rev. Lett.* **132**, 106601 (2024).
  - [12] S. Lai, H. Liu, Z. Zhang, J. Zhao, X. Feng, N. Wang, C. Tang, Y. Liu, K. S. Novoselov, S. Y. A. Yang, and W.-B. Gao, *Nat. Nanotechnol.* **16**, 869 (2021).
  - [13] M. M. Wei, L. Y. Wang, B. Wang, L. J. Xiang, F. M. Xu, B. G. Wang, and Jian Wang, *Phys. Rev. Lett.* **130**, 036202 (2023).
  - [14] L. J. Xiang, B. Wang, Y. D. Wei, Z. H. Qiao, and J. Wang, *Phys. Rev. B* **109**, 115121 (2024).
  - [15] J. E. Moore and J. Orenstein, *Phys. Rev. Lett.* **105**, 026805 (2010).
  - [16] Q. Ma, A. G. Grushin, and K. S. Burch, *Nat. Mater.* **20**, 1601, (2021).
  - [17] Q. Ma, R. K. Kumar, S.-Y., Xu, F. H. L. Koppens, and J. C. W. Song, *Nat. Rev. Phys.* **5**, 170 (2023).
  - [18] Y. Tokura and N. Nagaosa, *Nat. Commun.* **9**, 3740 (2018).
  - [19] J. Ahn, G.-Y. Guo, and N. Nagaosa, *Phys. Rev. X* **10**, 041041 (2020).
  - [20] J. Ahn, G.-Y. Guo, N. Nagaosa, and A. Vishwanath, *Nat. Phys.* **18**, 290 (2022).
  - [21] Päivi Törmä, *Phys. Rev. Lett.* **131**, 240001 (2023).
  - [22] P. C. Adak, S. Sinha, A. Agarwal, and M. M. Deshmukh, *Nat. Rev. Mater.* (2024).
  - [23] H. Wang, K. Chang, [arXiv:2405.13355](https://arxiv.org/abs/2405.13355).
  - [24] J. Sinova, D. Culcer, Q. Niu, N. A. Sinitsyn, T. Jungwirth, and A. H. MacDonald, *Phys. Rev. Lett.* **92**, 126603 (2004).
  - [25] C. Xiao, H. Liu, W. Wu, H. Wang, Q. Niu, and S. Y. A. Yang, *Phys. Rev. Lett.* **129**, 086602 (2022).
  - [26] C. Xiao, W. Wu, H. Wang, Y.-X. Huang, X. Feng, H. Liu, G.-Y. Guo, Q. Niu, and S. Y. A. Yang, *Phys. Rev. Lett.* **130**, 166302 (2023).

- [27] Y. Dai, J. Xiong, Y. Ge, B. Cheng, L. Wang, P. Wang, Z. Liu, S. Yan, C. Zhang, X. Xu, Y. Shi, S.-W. Cheong, C. Xiao, S. Y. A. Yang, S.-J. Liang, and F. Miao, *Nat. Commun.* **15**, 1129 (2024).
- [28] X. Feng, W. Wu, H. Wang, W. Gao, L. K. Ang, Y. X. Zhao, C. Xiao, and S. Y. A. Yang, *arXiv:2402.00532*.
- [29] J. Sinova, S. O. Valenzuela, J. Wunderlich, C. Back, and T. Jungwirth, *Rev. Mod. Phys.* **87**, 1213 (2015).
- [30] Y. Sun, Y. Zhang, C. Felser, and B. H. Yan, *Phys. Rev. Lett.* **117**, 146403 (2016).
- [31] I. Žutić, J. Fabian, and S. Das Sarma, *Rev. Mod. Phys.* **76**, 323 (2004).
- [32] M. Z. Hasan and C. L. Kane, *Rev. Mod. Phys.* **82**, 3045 (2010).
- [33] X.-L. Qi and S.-C. Zhang, *Rev. Mod. Phys.* **83**, 1057 (2011).
- [34] D. Xiao, J. Shi, D. P. Clougherty, and Q. Niu, *Phys. Rev. Lett.* **102**, 087602 (2009).
- [35] Y. Gao, S. Y. A. Yang, and Qian Niu, *Phys. Rev. Lett.* **112**, 166601 (2014).
- [36] H. Liu, J. Zhao, Y.-X. Huang, W. Wu, X. Sheng, C. Xiao, and S. A. Yang, *Phys. Rev. Lett.* **127**, 277202 (2021).
- [37] S. B. Zhang, C. A. Li, F. Pena-Benitez, P. Surowka, R. Moessner, L. W. Molenkamp, and B. Trauzettel, *Phys. Rev. Lett.* **127**, 076601 (2021).
- [38] F. Freimuth, S. Blügel, and Y. Mokrousov, *Phys. Rev. B* **90**, 174423 (2014).
- [39] M. Kimata, H. Chen, K. Kondou, S. Sugimoto, P. K. Muduli, M. Ikhlas, Y. Omori, T. Tomita, A. H. MacDonald, S. Nakatsuji, and Otani, *Nature* **565**, 627 (2019).
- [40] Y. Dai, J. Xiong, Y. Ge, B. Cheng, L. Wang, P. Wang, Z. Liu, S. Yan, C. Zhang, X. Xu, Y. Shi, S.-W. Cheong, C. Xiao, S. Y. A. Yang, S.-J. Liang, and F. Miao, *Nat. Commun.* **15**, 1129 (2024).
- [41] A. Roy, M. H. D. Guimarães, and J. Sławińska, *Phys. Rev. Mater.* **6**, 045004 (2022).
- [42] The MPGs that respecting  $\mathcal{PT}$ -symmetry ( $-1'$ ) are  $\bar{1}'$ ,  $2'/m$ ,  $2'/m'$ ,  $m'mm$ ,  $m'm'm'$ ,  $4/m'$ ,  $4'/m'$ ,  $4'/m'mm$ ,  $4'/m'm'm$ ,  $4'/m'm'm'$ ,  $\bar{3}'$ ,  $\bar{3}'m$ ,  $\bar{3}'m'$ ,  $6'/m$ ,  $6'/m'$ ,  $6'/m'mm$ ,  $6'/mmm'$ ,  $6'/m'm'm'$ ,  $m'\bar{3}'$ ,  $m'\bar{3}'m$ , and  $m'\bar{3}'m'$ .
- [43] D. Kaplan, T. Holder, and B.-H. Yan, *Phys. Rev. Lett.* **132**, 026301 (2024).
- [44] Supplemental Material.